Lithos 150 (2012) 26–36

Contents lists available at SciVerse ScienceDirect

Lithos

journal homepage: www.elsevier.com/locate/lithos

# A-type granite belts of two chemical subgroups in central eastern China: Indication of ridge subduction

He Li [a,d], Ming-xing Ling [a], Cong-ying Li [a,d], Hong Zhang [a,b], Xing Ding [a], Xiao-yong Yang [c], Wei-ming Fan [a], Yi-liang Li [e], Wei-dong Sun [b,*]

[a] State Key Laboratory of Isotope Geochemistry, Guangzhou Institute of Geochemistry, Chinese Academy of Sciences, Guangzhou 510640, China
[b] CAS Key Laboratory of Mineralogy and Metallogeny, Guangzhou Institute of Geochemistry, Chinese Academy of Sciences, Guangzhou 510640, China
[c] CAS Key Laboratory of Crust-Mantle Materials and Environments, School of Earth and Space Sciences, University of Science and Technology of China, Hefei 230026, China
[d] Graduate University of Chinese Academy of Sciences, Beijing 100049, China
[e] Department of Earth Sciences, University of Hong Kong, Pokfulam Road, Hong Kong, China

ARTICLE INFO

*Article history:*
Received 5 June 2011
Accepted 27 September 2011
Available online 6 October 2011

*Keywords:*
A-type granite
Ridge subduction
Adakite
Slab window
Mantle metasomatism
Lower Yangtze River belt

ABSTRACT

Early Cretaceous A-type granites in the Lower Yangtze River belt, central eastern China, with both $A_1$ and $A_2$ chemical subgroups, formed at $125 \pm 2$ Ma, after a Cretaceous ridge subduction. Remarkably, $A_1$ and $A_2$ group granites are distributed in three zones, roughly parallel to each other and to a slightly older adakite belt. In general, $A_1$ granites form in intraplate settings, whereas $A_2$ granites near paleo-convergent margins. The alternate distribution of these two subgroup A-type granites is compatible with a proposed Cretaceous ridge subduction in the region. The subduction of a dry and hot spreading ridge may have only released small amount of fluids, so that metasomatism on the overriding lithosphere was undetectable, correspondingly resulted in $A_1$ granites later on. In contrast, wetter and colder oceanic crust away from the spreading ridge was responsible for mantle metasomatism and consequently the formation of $A_2$ granites. Further away from the ridge, the subduction angle was much steeper, and dehydration of the slab had occurred earlier during the subduction, and thus dramatically reduced mantle metasomatism, corresponding to $A_1$ granites again. Both $A_1$ and $A_2$ granites formed within a short period of time due to slab window/rollback, after the ridge subduction. The distribution of the $A_1$ and $A_2$ granites together with the adakite belt may be taken as discrimination indice for ancient ridge subduction.



## 1. Introduction

The Lower Yangtze River (LYR) metallogenic belt, which extends from Wuhan in Hubei province in the west to Zhenjiang in Jiangsu province in the east, is an important metallogenic belt in eastern China (Chang et al., 1991; Deng et al., 2002; Pan and Dong, 1999; Xing, 1999; Zhai et al., 1992, 1996). Most of the deposits in the LYR belt formed in the Early Cretaceous ($140 \pm 5$ Ma) (Mao et al., 2006; Sun et al., 2003; Yang et al., 2007), and are closely associated with adakites of the same ages (Liu et al., 2010a; Wang et al., 2004, 2006, 2007; Xu et al., 2002; Zhang et al., 2001). Much attention has been paid on the geological evolution of this region (Chen et al., 2001; Ling et al., 2009; Sun et al., 2007; Xing and Xu, 1995). In addition to the adakite, there are a large number of the Early Cretaceous A-type granites along both banks of the LYR (Li et al., 2011; Wong et al., 2009; Xing and Xu, 1994; Zhang et al., 1988). The age distribution and formation mechanism of these A-type granites are important for understanding the geological evolution of the LYR belt.

The genesis of A-type granites in the LYR belt remains controversial. A-type granite is anhydrous, alkalic and anorogenic, which generally indicates formation in an extensional environment (Bonin, 2007; Eby, 1990, 1992; Loiselle and Wones, 1979). The extensional environment in the Early Cretaceous along the LYR belt was proposed to be either back-arc/post-collision extension settings (Cao et al., 2008; Du et al., 2007), or intracontinental shearing associated with mantle upwelling (Fan et al., 2008). Alternatively, it has been attributed to slab roll-back of the subducting Pacific plate (Wong et al., 2009) or a slab window induced by a ridge subduction (Ling et al., 2009).

In this contribution, we present the geochemical compositions and zircon ages of Maotan, Huayuangong, Xiangshuijian, Banshiling A-type granites on the south bank of the LYR. These together with previously published results are important to better understand the genesis of A-type granites and to constrain the geological evolution of the LYR belt.

## 2. Geological background

The LYR belt is situated in the east part of the Yangtze block, central eastern China (Fig. 1). Late Mesozoic igneous rocks widely

* Corresponding author. Tel.: +86 20 85290215.
*E-mail address:* weidongsun@gig.ac.cn (W. Sun).

0024-4937/$ – see front matter © 2011 Elsevier B.V. All rights reserved.
doi:10.1016/j.lithos.2011.09.021

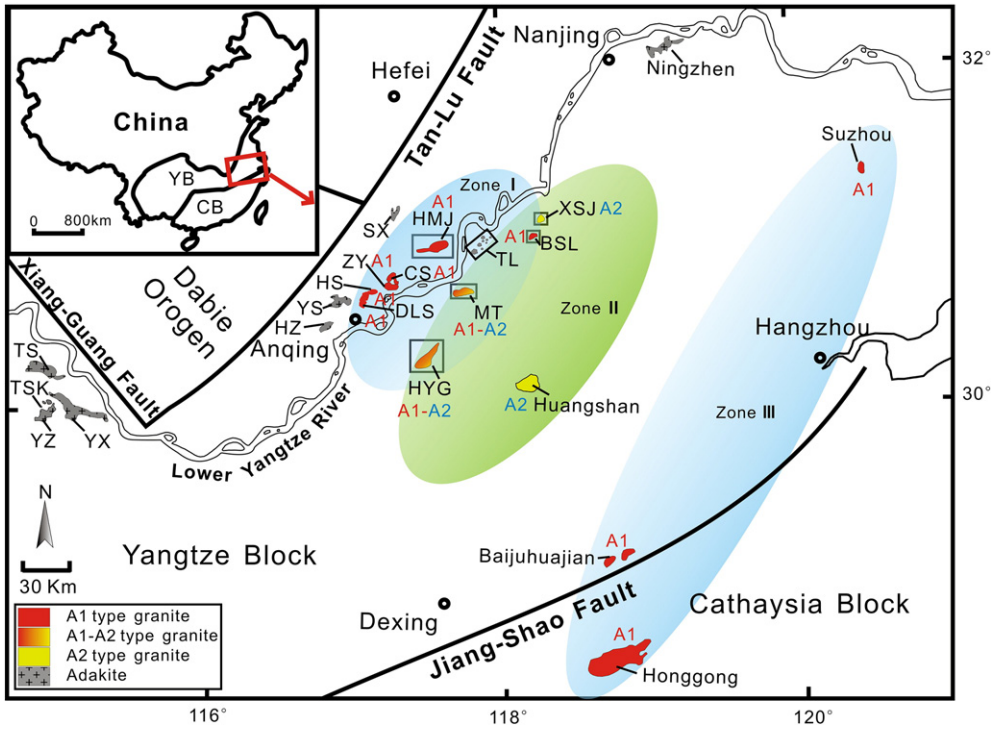


**Fig. 1.** Geological map of the Lower Yangtze River (LYR) belt. All the granites can be classified into three zones. DLS (Dalongshan), HS (Huashan), ZY (Zongyang), CS (Chengshan), HMJ (Huangmeijian) granites on the north bank of the LYR compiled from Fan et al. (2008) and Li et al. (2011) and BSL (Banshiling) on the south bank of the LYR are $A_1$-type granites near the Tan–Lu (Tancheng–Lujiang) fault forming zone I in the map; HYG (Huayuangong), MT (Maotan) granites on the south bank of the LYR have both $A_1$ and $A_2$ chemical group granites; Huangshan granite compiled from Xue et al. (2009) and Zhang et al. (2009) and XSJ (Xiangshuijian) granites are $A_2$ type granites in the zone II of the map; Suzhou, Baijuhuajian, and Honggong granites in zone III of the map are $A_1$-type granites near the Jiang-shao (Jiangshan-Shaoxing) fault (Wong et al., 2009). Adakites in the zone I contain TS (Tieshan), TSK (Tongshankou), YZ (Yinzu), and YX (Yangxin) compiled from Li et al. (2009) and Wang et al. (2004), YS (Yueshan) and HZ (Hongzhen) compiled from Wang et al. (2004), SX (Shaxi) (Yu et al., 2008), Ningzhen (Xu et al., 2002), and TL (Tongling) (Xie et al., 2009).

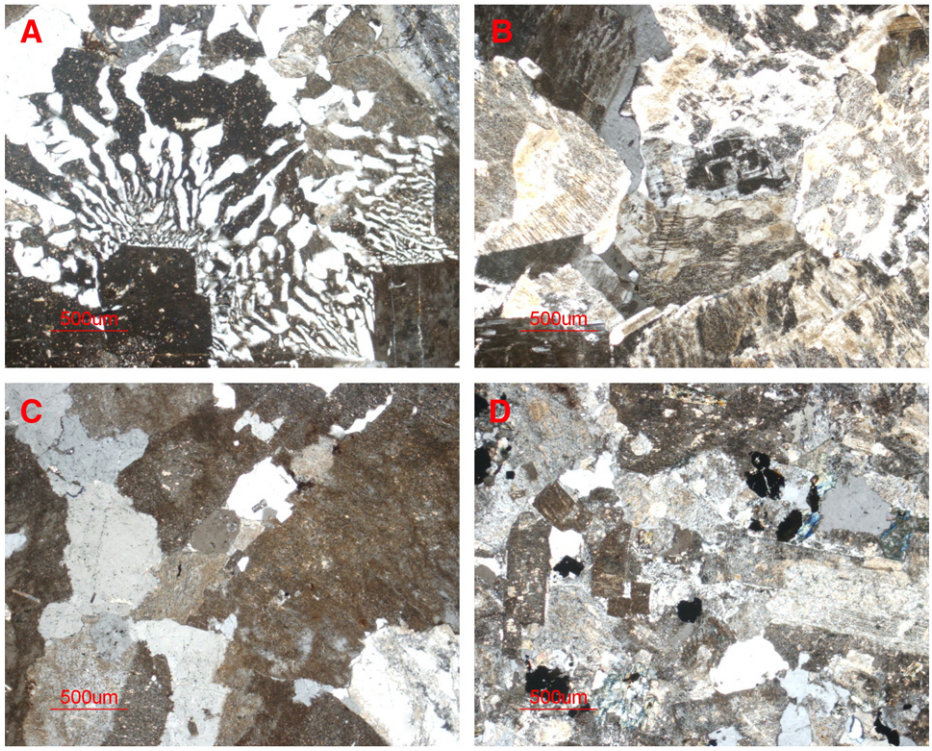


**Fig. 2.** A is a microscope photograph of the Maotan granite graphic texture (MT-9); B, C, and D are the individually microscope photographs of the Huayuangong granite (HYG-3), Xiangshuijian granite (XSJ-9) and Banshiling granite (BSL-9).

outcrop in the LYR belt. These igneous rocks intruded into Neoproterozoic low-grade metamorphic rocks and Paleozoic–Triassic sedimentary strata, and have been classified into three associations: Na-rich alkaline mafic, K-rich and high potassium calc-alkaline associations (Chang et al., 1991).

The LYR belt has been divided into three associated belts: the inner, the north and the south outer belts, according to tectonic, magmatic and metallogenic characteristics (Xing, 1999; Xing and Xu, 1995). The inner belt, distributed along both banks of the LYR, has intense mineralizations of Cu, Fe, S and Au, such as porphyry, skarn and stratabound type deposits (Hou et al., 2007; Pan and Dong, 1999; Xie et al., 2009), which are usually closely associated with the adakites (Ling et al., 2009; Wang et al., 2004, 2006, 2007; Xu et al., 2002; Zhang et al., 2004). The north outer belt has Cu deposits, e.g., the Shaxi Cu deposit (Yang et al., 2007, 2011; Yu et al., 2008). The south outer belt contains mainly porphyry type Mo, Cu and Pb–Zn deposits (Mao et al., 2006; Xing, 1999).

There are more than 10 A-type granite plutons in the LYR belt, e.g., Huashan, Zongyang, Chengshan (Fan et al., 2008) and Huangmeijian (Li et al., 2011) on the north bank, and Huayuangong, Maotan, Banshiling and Xiangshuijian on the south bank of the LYR, as well as Huangshan (Xue et al., 2009; Zhang et al., 2009), Suzhou (Wang et al., 1993, 1997), Baijuhuajian (Wong et al., 2009), and Honggong (Chen et al., 1991) further to the south.

The Maotan granite (30°41.70 N, 117°47.28E) is situated to the southwest of the Maotan town, Chizhou city in Anhui Province. It intruded into Silurian aleuvite and Devonian quartz sandstone with a granite outcrop area of about 25 $km^2$ (Wu and Zhou, 1998). It belongs to alkaline feldspar granite or quartz–syenite with granitic, porphyritic and graphic textures (Fig. 2A), and consists of quartz (7–22%), potassium feldspar (76–79%), plagioclase (1–4%), and biotite (0.5–3%).

The Huayuangong granite (30°37.58 N, 117°36.33E), located near Maya reservoir in Chizhou city, Anhui province, intruded into the Upper and Middle Cambrian sedimentary rocks on the south bank of the LYR (Xing and Xu, 1994). The granite is a medium- to fine-grained alkali feldspar granite with miarolitic texture, composed of quartz (25–33%), potassium feldspar (64–67%), plagioclase (2.5–3%), and biotite (<1%) (Fig. 2B).

The Xiangshuijian granite (31°02.23 N, 118°13.70E) is an alkali feldspar granite situated at the southeastern part of the Fanchang Basin, and consists of quartz (22–28%), potassium feldspar (64–67%), plagioclase (2–3%), and biotite (5–8%) (Fig. 2C).

The Banshiling granite (31°07.38 N, 118°17.65E) with an outcrop area of about 16 $km^2$ is situated at the southeastern part of the Fanchang Basin (Lou and Du, 2006). The surrounding rocks are Triassic sediments in the southeast and Permian sediments in the east and the north. It is a quartz monzonite, containing quartz (12–14%), potassium feldspar (43–48%), plagioclase (30–40%), and biotite (5–8%) (Fig. 2D).

**Table 1**
Representative major and trace element results of the Early Cretaceous A-type granites of the LYR belt.

| Sample | Maotan | | | Huayuangong | | | Xiangshuijian | | Banshiling | |
|---|---|---|---|---|---|---|---|---|---|---|
| | MT-3 | MT-4 | MT-12 | HYG-1 | HYG-8 | HYG-9 | XSJ-4 | XSJ-5 | BSL-4 | BSL-9 |
| $SiO_2$ | 74.8 | 75.6 | 71.4 | 74.6 | 74.5 | 74.1 | 72.5 | 72.4 | 63.9 | 63.7 |
| $TiO_2$ | 0.13 | 0.14 | 0.34 | 0.21 | 0.10 | 0.20 | 0.30 | 0.29 | 0.64 | 0.69 |
| $Al_2O_3$ | 13.0 | 12.6 | 14.3 | 13.6 | 13.9 | 13.2 | 13.4 | 13.4 | 15.9 | 15.9 |
| $Fe_2O_3$ | 1.29 | 1.22 | 1.82 | 1.46 | 2.04 | 1.84 | 1.78 | 1.70 | 3.94 | 4.21 |
| MnO | 0.01 | 0.01 | 0.02 | 0.01 | 0.01 | 0.19 | 0.09 | 0.10 | 0.09 | 0.11 |
| MgO | 0.07 | 0.00 | 0.21 | 0.07 | 0.04 | 0.01 | 0.18 | 0.19 | 0.68 | 0.99 |
| CaO | 0.43 | 0.24 | 0.40 | 0.33 | 0.22 | 0.22 | 0.55 | 0.83 | 2.02 | 1.97 |
| $Na_2O$ | 3.64 | 3.87 | 4.07 | 4.01 | 3.88 | 4.38 | 4.09 | 3.77 | 2.70 | 2.83 |
| $K_2O$ | 5.34 | 5.28 | 6.11 | 4.78 | 4.67 | 5.03 | 5.30 | 5.53 | 6.71 | 6.26 |
| $P_2O_5$ | 0.01 | 0.01 | 0.04 | 0.02 | 0.01 | 0.02 | 0.02 | 0.02 | 0.27 | 0.31 |
| L.O.I | 0.56 | 0.60 | 0.88 | 0.53 | 0.31 | 0.48 | 1.37 | 1.21 | 2.90 | 2.78 |
| Total | 99.3 | 99.6 | 99.6 | 99.6 | 99.6 | 99.6 | 99.6 | 99.5 | 99.7 | 99.7 |
| $K_2O/Na_2O$ | 1.46 | 1.36 | 1.50 | 1.19 | 1.21 | 1.15 | 1.30 | 1.47 | 2.48 | 2.22 |
| Fe-number | 0.94 | 1.00 | 0.89 | 0.95 | 0.98 | 0.99 | 0.90 | 0.89 | 0.84 | 0.79 |
| Rb | 257 | 203 | 24.5 | 93.4 | 216 | 215 | 206 | 206 | 197 | 202 |
| Sr | 28.5 | 13.8 | 304 | 57.5 | 16.7 | 41.0 | 76.1 | 103 | 232 | 276 |
| Y | 38.4 | 34.9 | 18.8 | 49.0 | 26.2 | 44.0 | 60.2 | 63.9 | 24.0 | 25.6 |
| Zr | 213 | 201 | 100 | 145 | 157 | 255 | 375 | 407 | 345 | 353 |
| Nb | 51.7 | 40.5 | 4.20 | 11.6 | 40.2 | 47.7 | 33.2 | 32.8 | 21.5 | 21.6 |
| Ba | 41.2 | 47.7 | 91.7 | 97.3 | 59.9 | 109 | 129 | 125 | 859 | 817 |
| La | 38.8 | 43.0 | 15.6 | 27.2 | 39.8 | 58.2 | 80.4 | 86.2 | 75.0 | 58.2 |
| Ce | 66.4 | 73.8 | 35.0 | 72.7 | 66.9 | 114 | 138 | 153 | 132 | 104 |
| Pr | 6.78 | 8.80 | 4.12 | 9.07 | 6.38 | 11.5 | 14.9 | 16.3 | 13.3 | 10.7 |
| Nd | 18.7 | 25.7 | 15.9 | 37.9 | 18.1 | 34.1 | 59.3 | 65.4 | 48.7 | 42.0 |
| Sm | 3.18 | 4.65 | 3.20 | 9.06 | 2.96 | 5.80 | 11.7 | 12.7 | 7.43 | 6.67 |
| Eu | 0.21 | 0.29 | 0.83 | 2.00 | 0.26 | 0.46 | 0.92 | 0.90 | 1.46 | 1.43 |
| Gd | 3.04 | 4.18 | 3.12 | 8.96 | 2.88 | 5.09 | 10.5 | 11.3 | 5.92 | 5.38 |
| Tb | 0.62 | 0.76 | 0.52 | 1.49 | 0.48 | 0.88 | 1.61 | 1.70 | 0.72 | 0.79 |
| Dy | 4.36 | 4.59 | 2.94 | 8.27 | 3.11 | 5.78 | 10.5 | 11.2 | 4.27 | 4.59 |
| Ho | 1.02 | 0.99 | 0.58 | 1.63 | 0.71 | 1.27 | 2.14 | 2.32 | 0.92 | 0.92 |
| Er | 3.71 | 3.42 | 1.70 | 4.49 | 2.50 | 4.24 | 6.47 | 6.84 | 2.58 | 2.73 |
| Tm | 0.68 | 0.59 | 0.25 | 0.61 | 0.45 | 0.73 | 0.94 | 1.01 | 0.37 | 0.43 |
| Yb | 5.29 | 4.49 | 1.68 | 3.97 | 3.58 | 5.50 | 6.89 | 7.24 | 3.12 | 3.06 |
| Lu | 0.90 | 0.77 | 0.25 | 0.60 | 0.63 | 0.89 | 1.00 | 1.07 | 0.46 | 0.47 |
| Hf | 8.79 | 7.52 | 2.77 | 4.30 | 7.26 | 9.55 | 11.1 | 11.4 | 8.40 | 8.45 |
| Ta | 3.19 | 2.71 | 0.35 | 0.97 | 2.61 | 3.30 | 2.20 | 2.23 | 1.56 | 1.47 |
| Th | 45.9 | 27.9 | 5.0 | 12.6 | 31.9 | 38.7 | 25.6 | 24.0 | 22.6 | 18.8 |
| Y/Nb | 0.74 | 0.86 | 4.49 | 4.24 | 0.65 | 0.92 | 1.81 | 1.95 | 1.12 | 1.19 |
| Type | $A_1$ | $A_1$ | $A_2$ | $A_2$ | $A_1$ | $A_1$ | $A_2$ | $A_2$ | $A_1$ | $A_1$ |

$A_1$ represents $A_1$ type granite and $A_2$ represents $A_2$ type granite (wt. % for major element unit and ppm for trace element unit).

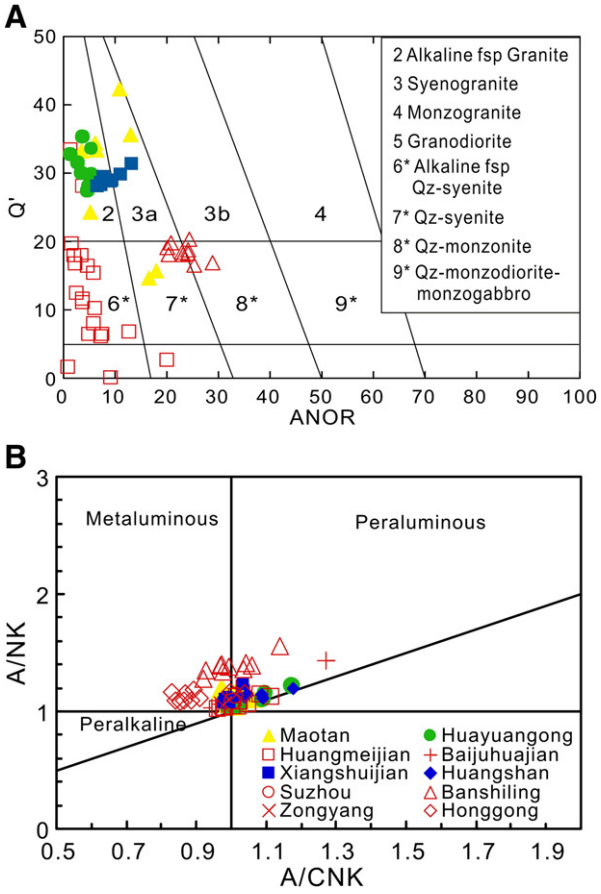


**Fig. 3.** (A) Rock discrimination diagram for the LYR belt granites. ANOR = An/(Or + An) * 100; Q′ = Q/(Q + Or + Ab + An) (Streckeisen and Le Maitre, 1979) (symbols as in Fig. 3B). (B) A/NK versus A/CNK diagram for the LYR belt granites. Most of the granites show a metaluminous–peraluminous nature. A/NK = Al/(Na + K) (molar ratio). A/CNK = Al/(Ca + Na + K) (molar ratio).

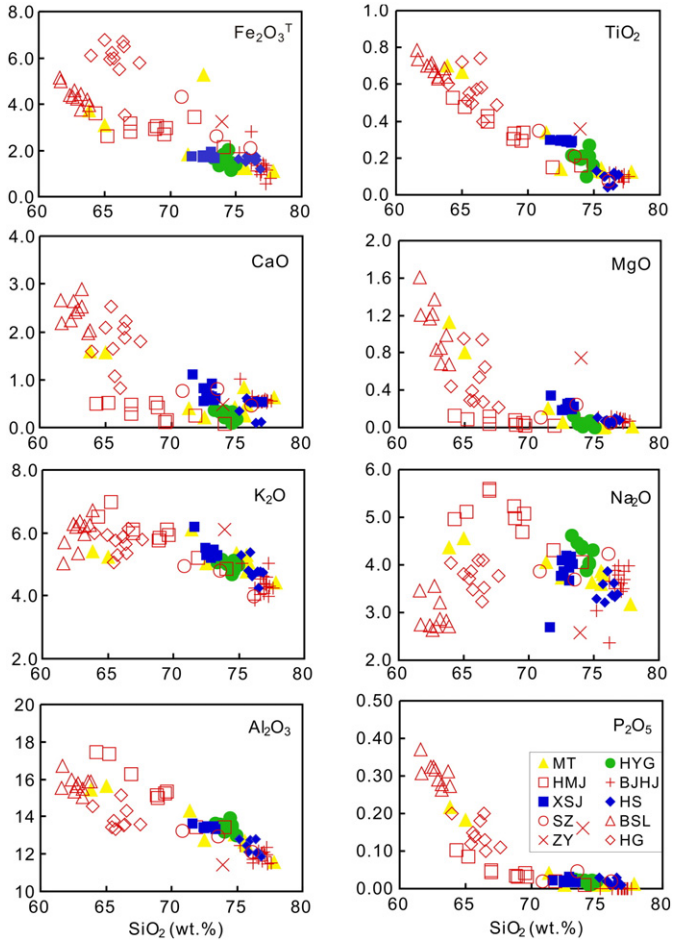


**Fig. 4.** Harker diagrams for the granites in the LYR belt.

## 3. Analytical methods

### 3.1. Whole-rock major and trace element analyses

The major and trace elements of the bulk rock samples were analyzed at the State Key Laboratory of Isotope Geochemistry, Guangzhou Institute of Geochemistry, Chinese Academy of Sciences. Whole rock samples were first powdered to less than 200 mesh, and then fluxed with $Li_2B_4O_7$ (1:8) to make homogeneous glass disks at 1150–1200 °C using a V8C automatic fusion machine produced by the Analymate Company in China. The bulk rock major elements were analyzed using X-ray fluorescence spectrometry (Rigaku 100e). The analytical precisions for major elements were better than 1% (Li et al., 2005).

The trace element analyses of samples from Banshiling and Xiangshuijian were carried out using fluxed glass disks (with sample to $Li_2B_4O_7$ ratio of 1:3) at 1150–1200 °C using a V8C automatic fusion machine, and then analyzed at the State Key Laboratory of Isotope Geochemistry, Guangzhou Institute of Geochemistry, Chinese Academy of Sciences using LA–ICPMS. The LA–ICPMS system is composed of an Agilent 7500a ICP-MS coupled with a Resonetic RESOLution M-50 ArF-Excimer laser source (λ = 193 nm). Laser energy was 80 mJ, with repetition rate of 6 Hz, spot size of 69 μm in diameter and a total of 40 s ablation time. Both a double-volume sampling cell and Squid pulse smoothing device were used to improve data quality (Liang et al., 2009; Tu et al., 2011). Helium gas was used as carrier gas to the ICP source. NIST610 was used as an external calibration standard, and $^{29}Si$ as an internal standard. The whole rock trace element data were calculated by ICPMSDataCal 7.0 (Liu et al., 2008).

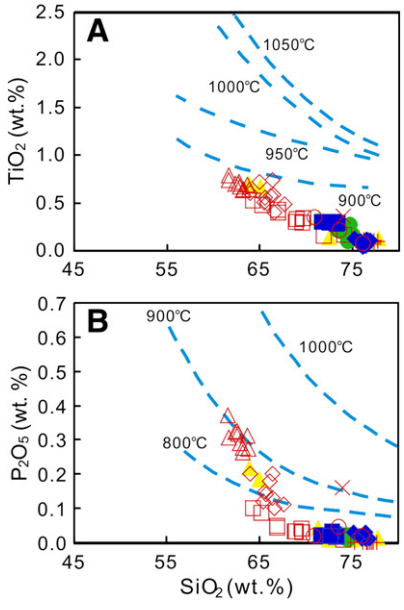


**Fig. 5.** (A) $TiO_2$ vs $SiO_2$ diagram for the granites in the LYR belt (Green and Pearson, 1986). (B) $P_2O_5$ vs $SiO_2$ diagram for the granites in the LYR belt (Harrison and Watson, 1984) (symbols as in Fig. 4).

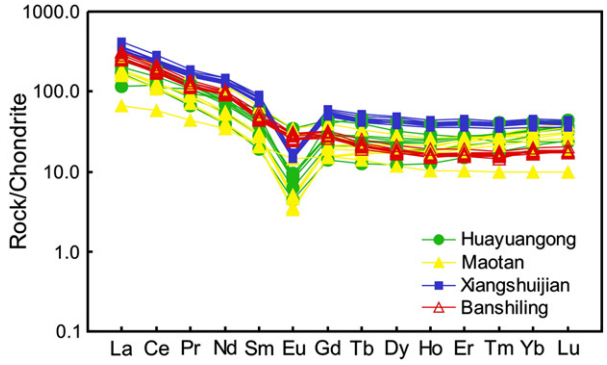


**Fig. 6.** Chondrite-normalized REE diagram for the granites in the LYR belt. Chondritic values are from Sun and McDonough (1989).

For trace element analyses of Maotan and Huayuangong plutons, 200 mesh sample pulps were first digested with a mixture of HF and $HNO_3$ acids in screw-top PTFE-lined stainless steel bombs at 185 °C for two days, and insoluble residues were dissolved in $HNO_3$ acid heated to 145 °C for 3 h to ensure complete digestion. Pure Rh standard solutions were used for internal calibration and GSR-1, BHVO-1 and OU-6 were used as reference materials. Bulk rock trace elements were analyzed using ICP-MS, with accuracies of better than 5% for most elements, as indicated by multiple analyses of standards (Liu et al., 1996).

### 3.2. Zircon U–Pb dating and zircon trace element analyses

Zircon grains were first separated through powdering samples to about 60 mesh, desliming in water, followed by density separation, magnetic separation and handpicking, then mounted in epoxy and polished down to nearly a half section to expose internal structures. Cathodoluminescent and optical microscopy images were taken in order to ensure that the least fractured, inclusion-free zones in zircon were analyzed. Zircon U–Pb dating and trace elements were analyzed using the same LA–ICPMS system described above. The conditions were 80 mJ laser energy and a repetition rate of 10 Hz with spot a size of 31 μm in diameter and 40 s ablation time. Helium was used as carrier gas sampling ablation aerosols to the ICP source. NIST610 and TEM were used as an external calibration standard, and $^{29}Si$ as the internal standard. The calculations of zircon isotope ratios and zircon trace elements were performed by ICPMSDataCal 7.0 (Liu et al., 2008, 2010b). Zircon Ce anomalies were calculated using software from the Research School of Earth Sciences, Australian National University (Ballard et al., 2002; Liang et al., 2006) and the zircon age was calculated using Isoplot (Version 3.23).

## 4. Results

### 4.1. Whole-rock major and trace elements

Thirty-six samples were analyzed for major and trace element compositions, including eight samples from Maotan granite and Huayuangong granite each, ten samples from Xiangshuijian granite and Banshiling granite each. The major and trace element data are summarized in Tables 1 and A.1.

All the samples have high $SiO_2$, $Fe_2O_3^T$, $Na_2O + K_2O$ contents, high K/Na, Fe/Mg ratios and low $Al_2O_3$, $TiO_2$, MgO and CaO contents compared to adakite in the same region (Tables 1 and A.1). According to the Q'-ANOR diagram (Streckeisen and Le Maitre, 1979), the granites range in composition from alkali granite to alkali quartz syenite, syenogranite and quartz–syenite (Fig. 3A), and are metaluminous–peraluminous as shown in Fig. 3B. In the Harker diagrams, $SiO_2$ has obviously negative correlation with $Fe_2O_3^T$, $TiO_2$, MgO and CaO, but no correlation with $Na_2O$, $K_2O$ and $P_2O_5$ (Fig. 4). As shown in Fig. 5, all the granites formed at temperature of lower than 900 °C (Green and Pearson, 1986; Harrison and Watson, 1984). Two of the granites, Xiangshuijian and Huangshan, show lower temperatures.

Trace elements of the samples are characterized by having high concentrations of large ion lithophile elements (LILE) such as Na, K and Rb and high field strength elements (HFSE) such as Zr, Hf, Nb, Ta, rare earth elements (REE, except Eu) and Th (Tables 1 and A.1). According to the chondrite-normalized REE diagram, they are enriched in light rare earth elements (LREE) relative to heavy rare earth elements (HREE) and show negative Eu-anomalies (Fig. 6), which indicates removal of plagioclase by fractional crystallization during magma evolution. Consistently, negative anomalies in Ba, Sr, and Eu in the primitive mantle-normalized trace element diagram (Fig. 7) also suggest fractional crystallization of feldspars. The depletion of Ti coupled with high Nb, Ta concentrations suggests crystallization of ilmenite, with little influence of rutile or titanite. Ilmenite, rutile and titanite are the main Ti enriched minerals, with ilmenite stable at high temperature and low pressure (Liou et al., 1998). Rutile and titanite usually have high concentrations of Nb and Ta (Cole and Stewart, 2009; Foley et al., 2002; Green, 1995; Manning and Bohlen, 1991; Mcdonough, 1991; Rudnick et al., 2000; Xiong et al., 2005). In contrast, ilmenite usually has much lower Nb and Ta (Cole and Stewart, 2009; Ding et al., 2009). Thus, crystallization of ilmenite takes Ti out of the magma, leading to depletion of Ti in the granite without significant decreases of Nb and Ta. The crystallization of ilmenite is consistent with the high temperature characteristics of those granites.

Beside the common characteristics described above, a key difference of trace elements can be found among the granite samples. Maotan (except MT-12), Huayuangong (except HYG-1) and Banshiling granites have Y/Nb ratios lower than 1.2, while Xiangshuijian granite and two samples from Maotan and Huayuangong granite (MT-12 and HYG-1) have Y/Nb ratios higher than 1.2 (Table 1).

### 4.2. LA–ICPMS U–Pb zircon dating

Zircons from Maotan (two samples), Huayuangong (two samples), Xiangshuijian and Banshiling (one sample each) granites were analyzed and the zircons U–Pb isotopic data and trace elements are summarized in Tables A.2 and A.3, and illustrated in the concordia diagram and chondrite-normalized REE diagram (Figs. 8, 9).

All zircons are generally prismatic, colorless, transparent, and euhedral with obvious oscillatory zoning but no inherited cores in CL image, as well as Th/U values of 0.73–2.97, indicating a magmatic origin (Belousova et al., 2002; Hoskin and Black, 2000). The weighted mean $^{206}Pb/^{238}U$ ages for Maotan, Huayuangong, Banshiling and Xiangshuijian granites are individually 125.4 ± 2.2 Ma (MT-9), 125.4 ±

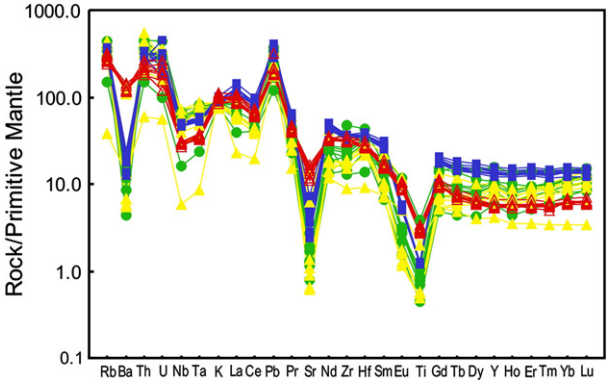


**Fig. 7.** Primitive mantle-normalized trace element diagram for the granites in the LYR belt. Primitive mantle values are from Sun and McDonough (1989) (symbols as in Fig. 6).

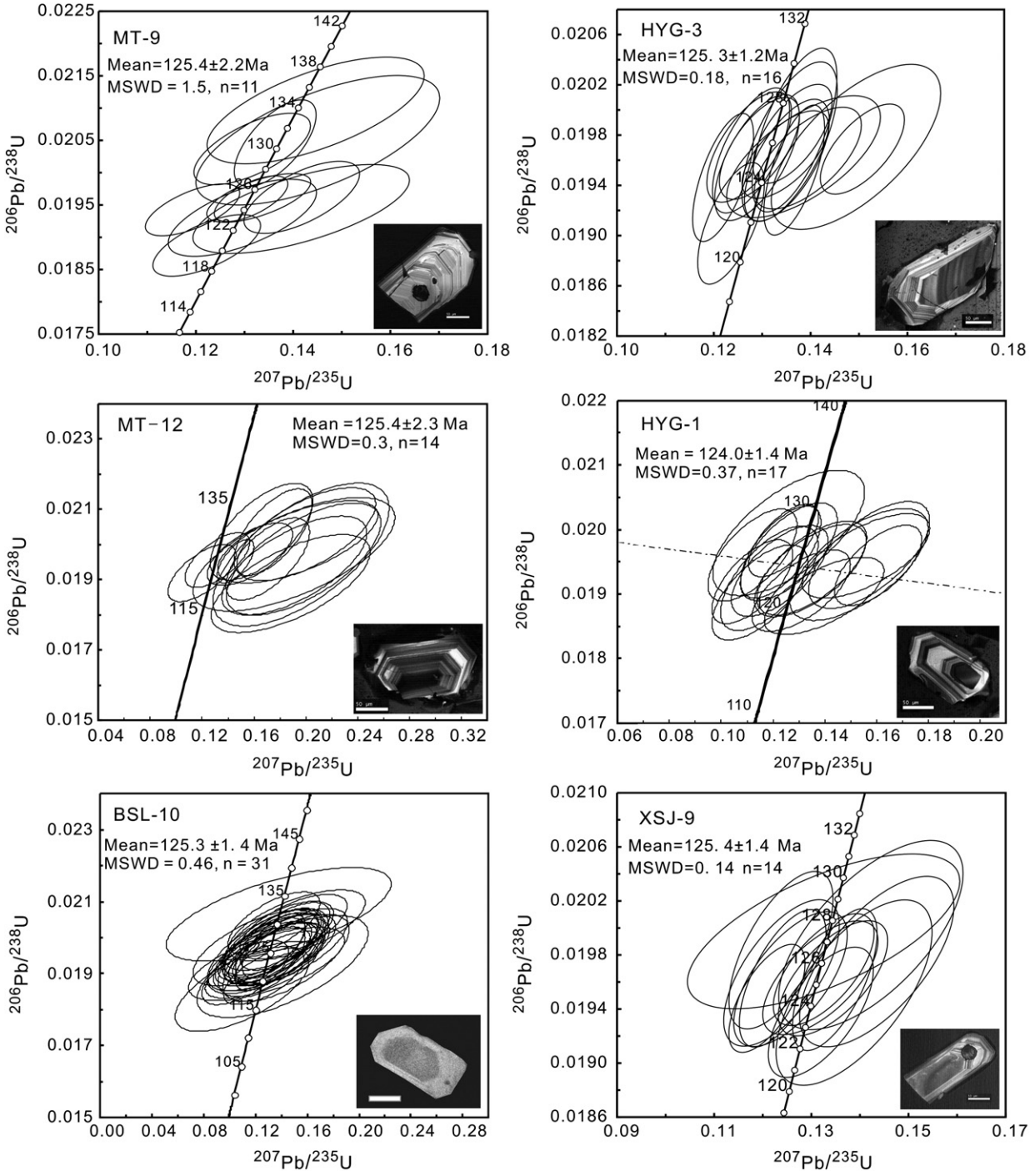


**Fig. 8.** Zircon U–Pb concordia diagram of granites from Maotan (MT-9 and MT-12), Huayuangong (HYG-3 and HYG-1), Banshiling (BSL-10) and Xiangshuijian (XSJ-9). The scale bar is 50 μm.

2.3 Ma (MT-12), 125.3 ± 1.2 Ma (HYG-3), 124.0 ± 1.4 Ma (HYG-1), 125.3 ± 1.4 Ma (BSL-10) and 125.4 ± 1.4 Ma (XSJ-9) (Fig. 8, Table A.2). All the A-type granites in the LYR belt were formed at 125 ± 2 Ma (Table 2).

Chondrite-normalized REE diagram shows negative Eu anomaly and positive Ce anomaly in most zircons (Fig. 9, Table A.3). Zircon Ce(IV)/Ce(III) ratios for sample Maotan (MT-9), Huayuangong (HYG-3) and Banshiling (BSL-10) granites are relatively lower than those of Xiangshuijian (XSJ-9) granite and each sample from Maotan and Huayuangong granites (MT-12 and HYG-1), which indicates the granites formed at low oxygen fugacity (Ballard et al., 2002; Liang et al., 2006) (Table A.2). According to Ti concentrations in zircons, the temperatures of zircon formation are high, ranging from 700 to 900 °C (Watson et al., 2006) (Table A.2). These temperatures are roughly consistent with the temperature estimated using major elements (Fig. 5) (Green and Pearson, 1986; Harrison and Watson, 1984).

## 5. Discussion

### 5.1. Two chemical subgroups of A-type granites

A-type granite stands for alkaline, anorogenic and anhydrous, characterized by enrichments of $Na_2O + K_2O$ and HFSE (e.g. Zr, Y,

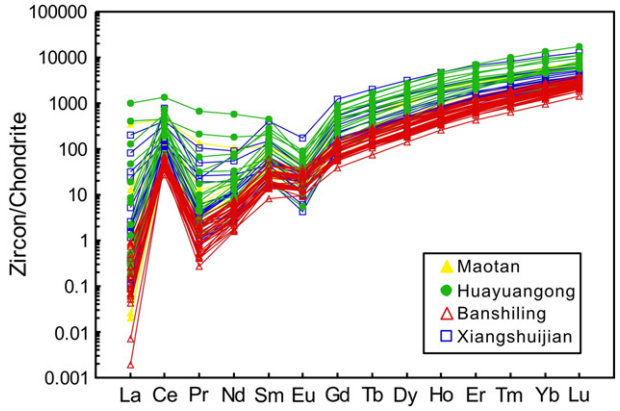


**Fig. 9.** Zircon chondrite-normalized REE diagram. Chondritic values are from Sun and McDonough (1989).

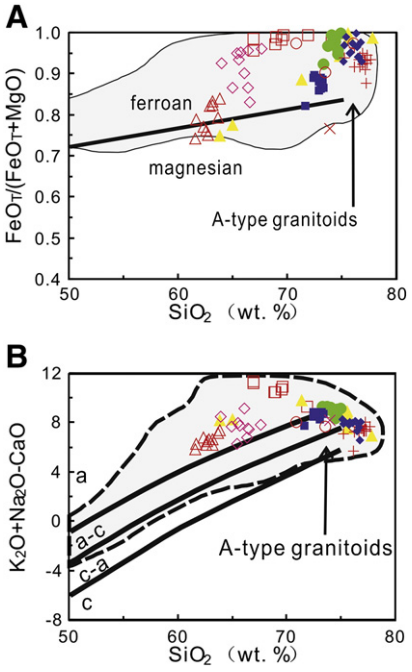


**Fig. 10.** Discrimination diagrams for A-type granites in the LYR belt, modified after Frost et al. (2001) and Frost and Frost (2011) (symbols as in Fig. 11).

Nb, Ce), high $FeO_T/(FeO_T + MgO)$, implying that many A-type granites are ferroan and all the studied granites in the LYR belt are A-type granites (Fig. 10) (Frost and Frost, 2011; Frost et al., 2001). A-type granite has been further divided into $A_1$ and $A_2$ chemical subgroups (Eby, 1992). $A_1$ granites have chemical characteristics similar to those observed for oceanic-island basalts, and are thus mantle derived at intraplate settings. In contrast, $A_2$ granites are similar to rocks of continental crust or island-arc origins in chemical characteristics, and are attributed to continental crust at convergent margins (Eby, 1992). Therefore, the arc signature of $A_2$ granites may be originally introduced through mantle metasomatism by subduction released fluids.

A-type granites located along the north bank of the LYR (Dalongshan, Huashan, Zongyang, Huangmeijian) and near the Jiangshao fault zone (Baijuhuajian, Honggong and Suzhou) are plotted in $A_1$ subgroup, overlap with the OIB field, i.e., formed at intraplate settings (Fig. 11). Xiangshuijian and Huangshan granites are classified as $A_2$ subgroup, indicating their affinities to convergent margin tectonic settings. Remarkably, the A-type granites along the south bank of the LYR belt (Maotan and Huayuangong) have significantly varied compositions, and are plotted in both $A_1$ and $A_2$ fields (Fig. 11).

Overall, $A_1$ and $A_2$ subgroup granites outcrop in the LYR belt are distributed in three zones, roughly parallel to each other and to an adakite belt along the LYR (Fig. 1). The adakite belt was formed within a short period of time at $140 \pm 5$ Ma (Li et al., 2009; Xie et al., 2006, 2007, 2008, 2009), and has been attributed to ridge subduction (Ling et al., 2009; Sun et al., 2010). In contrast, both $A_1$ and $A_2$ type granites from the LYR belt and nearby regions in central eastern China (Fig. 1), were formed at $125 \pm 2$ Ma (Table 2), systematically younger than the Cretaceous LYR adakites. These A-type granite belts of the same age indicate unique tectonic settings with both intraplate and convergent margin characteristics, which provide important constraints on the tectonic evolution of the LYR belt in the Early Cretaceous.

### 5.2. A-type granites and adakites in the LYRB

The mechanism for the formation of A-type granite in the LYR belt is controversial. It was once proposed that A-type granite in the LYR belt formed in back-arc and post-collisional extension settings related to the Triassic collision between the North and South China blocks (Cao et al., 2008; Du et al., 2007). The Triassic collision, however, occurred along the Qinling–Dabie–Sulu orogenic belt (Li et al., 1993, 2000; Sun et al., 2002; Zheng et al., 2003), while A-type granites distributed in the LYR belt (Xing and Xu, 1994) and also near the Jiangshao fault (Wong et al., 2009), several hundred kilometers to the east and south of the orogenic belt and more than 100 Ma after the collision. It is therefore, unrealistic to attribute A-type granites to Qinling–Dabie–Sulu orogen. The extensional environment was also attributed to an intracontinental shearing associated with mantle upwelling (Fan et al., 2008). This model, however, does not explain why

**Table 2**
Ages of A-type granites from the LYR belt.

| Pluton | Lithology | Age (Ma) | Method | Reference |
|---|---|---|---|---|
| Chengshan | Alkaline granite | $126.5 \pm 2.1$ | LA–ICPMS Zircon U–Pb | Fan et al. (2008) |
| Huashan | Quartz syenite | $126.2 \pm 0.8$ | LA–ICPMS Zircon U–Pb | Fan et al. (2008) |
| Huangmeijain | Quartz syenite | $125.4 \pm 1.7$ | LA–ICPMS Zircon U–Pb | Fan et al. (2008) |
| Zongyang | Alkaline granite | $124.8 \pm 2.2$ | LA–ICPMS Zircon U–Pb | Fan et al. (2008) |
| Huangmeijian | Quartz syenite | $125 \pm 4$ | Zircon U–Pb | Zheng et al. (1995) |
| Banshiling | Quartz monzonite | $125.3 \pm 2.9$ | SHRIMP Zircon U–Pb | Lou and Du (2006) |
| Suzhou | Feldspar granite | 123 | Ar–Ar whole rock | Chen et al. (1993) |
| Honggong | Quartz syenite | 124.5 | Ar–Ar biotite | Chen et al. (1991) |
| Huangmeijian | Alkaline feldspar quartz syenite | $127.1 \pm 1.4$ | LA–ICPMS Zircon U–Pb | Li et al. (2011) |
| Maotan | Alkaline feldspar granite | $125.4 \pm 2.2$ | LA–ICPMS Zircon U–Pb | This article |
| Huayuangong | Alkaline feldspar granite | $125.3 \pm 1.2$ | LA–ICPMS Zircon U–Pb | This article |
| Xiangshuijian | Alkaline feldspar granite | $125.4 \pm 1.4$ | LA–ICPMS Zircon U–Pb | This article |
| Banshiling | Quartz monzonite | $125.3 \pm 1.4$ | LA–ICPMS Zircon U–Pb | This article |

Data are collected from Chen et al. (1991, 1993), Fan et al. (2008), Li et al. (2011), Lou and Du (2006), and Zheng et al. (1995).

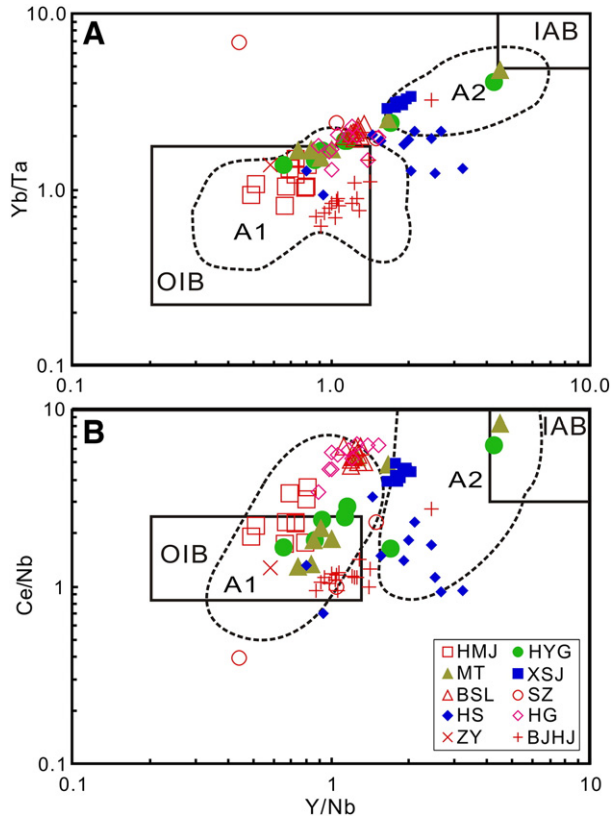


**Fig. 11.** (A) Yb/Ta versus Y/Nb and (B) Y/Nb versus Ce/Nb diagrams for the LYR belt A-type granites (Eby, 1992). OIB = oceanic island basalt; IAB = island arc basalt. Fields with dashed lines represent $A_1$- and $A_2$-type granites of Eby (Eby, 1990). HMJ (Huangmeijian), ZY (Zongyang), BSL (Banshiling), BJHJ (Baijuhuajian), HG (Honggong) and SZ (Suzhou) granites are plotted into $A_1$ group granite area; HYG (Huayuangong) and MT (Maotan) granites are plotted into Both $A_1$ and $A_2$ group granite areas; XSJ (Xiangshuijian) and HS (Huangshan) granites are plotted into $A_2$ group granite area.

mantle upwelling occurred within a short period of time (only 2–3 Ma) in the LYR belt and nearby region. None of these models explains why both $A_1$ and $A_2$ type granites occur in the LYR belt at $125 \pm 2$ Ma. Moreover, these models did not pay any attention to the adakites and other rocks of the Early Cretaceous in the region, which are spatially closely associated with, but systematically predate, A-type granites.

Adakitic rocks from the LYR belt were previously attributed to partial melting of either thickened or delaminated lower continental crust, mainly because their Nd isotope compositions are lower than that of typical MORB and the present geographic locations are far away from the current west Pacific subduction zones (Wang et al., 2007; Xu et al., 2002; Zhang et al., 2001). Geochemical studies indicate that the LYR adakites are slab melts, rather than lower continental crust melt. Moreover, partial melting of thickened lower continental crust cannot explain the high-Mg and Cu-enriched characteristics of these adakitic rocks (Ling et al., 2011). A delaminated lower continental crust, however, should presumably disturb the asthenosphere before being partially melted. In this case, A-type granites should be older than adakitic rocks, which is opposite to the observations so far available.

The Jiangshao fault is a Proterozoic suture between the Yangtze and Cathaysia blocks (Zhou et al., 1990). One may argue that the $A_2$ signature of granites in the LYR belt may have been inherited from the subduction at ~1.0 Ga. The A-type granites near the Jiangshao suture zone, however, are of $A_1$ affinity, which clearly indicates that the ancient suture zone had no detectable influence to the distribution of Cretaceous A-type granites in the region (Fig. 1).

### 5.3. Ridge subduction model

A ridge subduction model has been proposed to explain the geologic events in the LYR belt, based on the drifting history of the Pacific plate, and rock assemblages, e.g., adakite, Nb-enriched volcanic rocks and A-type granite, as well as Cu-polymetal deposits (Ling et al., 2009; Sun et al., 2010). According to the ridge subduction model, partial melting of the subducting young, hot oceanic crust close to the ridge formed adakitic rocks and associated Cu deposits, whereas A-type granitoids formed as a result of subsequent slab window opening. The distribution of A-type granites, especially the roughly parallel zones of $A_1$ and $A_2$ subgroup granites can be plausibly interpreted by the ridge subduction model as follows.

From the Late Jurassic to the Early Cretaceous, there were two plates subducting underneath eastern China, the Izanagi plate subducting northwestward (Maruyama et al., 1997), and the Pacific plate subducting southwestward (Sun et al., 2007; Wang et al., 2011). Because of the different directions and possibly also different rate of subduction between the Pacific and the Izanagi plates, the ridge between these two plates moved westward during the subduction, and subducted under the LYR region at about $140 \pm 5$ Ma (Ling et al., 2009, 2011; Sun et al., 2010). The ridge gradually opened as the subduction continued, possibly formed a slab window and consequently, A-type granites at ~125 Ma (Li et al., 2011; Ling et al., 2011).

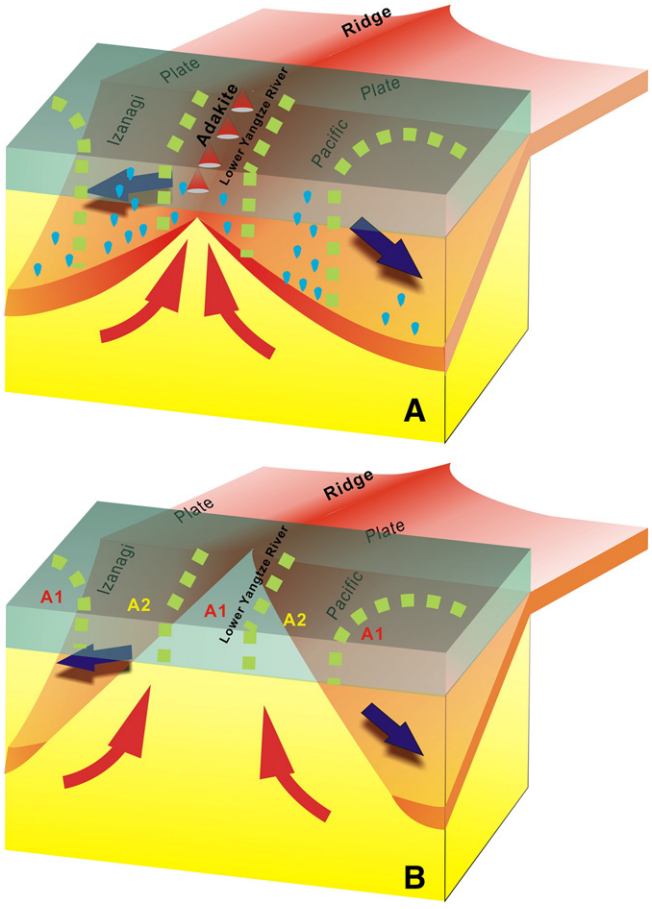


**Fig. 12.** (A) Ridge subduction model diagram. The Pacific plate was subducting toward the southwest (Sun et al., 2007), and the Izanagi plate was subducting toward the northwest (Maruyama et al., 1997). Due to the different directions and velocity between the Pacific and Izanagi plates, the ridge between the two plates moved westward during the subduction, and subducted under the Lower Yangtze River region at about 145 Ma or earlier. (B) Slab window model diagram. As the subduction continued, the ridge gradually opened, forming a slab window (Ling et al., 2009) and consequently, $A_1$- and $A_2$-type granites.

This slab window opening process may be coupled with the slab rollback process.

The asthenospheric mantle is characterized by dry and high temperatures. Previous studies on ridge subduction proposed that A-type granite associated with ridge subduction probably resulted from asthenospheric mantle upwelling through the slab window and evolved at shallow crust at a low pressure condition (Thorkelson and Breitsprecher, 2005).

The spreading ridge is hotter and drier than normal oceanic crust. Limited water hosted in oceanic crust near the ridge should mostly have been absorbed by adakitic magmas during dehydration melting of the subducting slab (Xiao et al., 2006) in the presence of ruitle (Xiong, 2006; Xiong et al., 2009, 2011), so that there was no significant dehydration induced metasomatism above the ridge (Fig. 12A). As a result, $A_1$ granites may form during the asthenosphere upwelling triggered by slab window opening and/or slab rollback. This explains why $A_1$ granites and adakitic rocks distributed roughly in the same region (Fig. 12B).

The oceanic crust becomes wetter and colder from the spreading ridge outwards. Therefore, dehydration induced metasomatism increases with decreasing adakitic magmas during the ridge subduction (Fig. 12A). Consequently, A-type granites formed during subsequent asthenosphere upwelling, changed gradually from $A_1$ to $A_2$ chemical signature (Fig. 12B). A-type granites formed near the adakite belt, have both $A_1$ and $A_2$ characteristics, which marks the turning point of subduction induced metasomatism (Fig. 1). Further to the south, the subduction angle was presumably much steeper, and dehydration of the slab had occurred early during the plate subduction. Consequently, the overriding continental lithosphere far away from the subduction zone was not intensively metasomatised by subduction released fluids. Therefore, A-type granites formed in this region are $A_1$ type again (Figs. 1, 12). Such alternate distribution of $A_1$ and $A_2$ granites, as well as their spatial association with slightly older adakitic rocks may be taken as discrimination indice, indicating ancient subduction of spreading ridges.

Early Cretaceous A-type granites are also distributed widely from Tan-Lu fault zone in the northwest to Jiangshao fault zone in the southeast in the LYR belt, and formed within only a short period of time (about 2–3 Ma), we proposed that slab roll back together with the ridge subduction may have played a major role in the formation of A-type granites in the LYR belt and the nearby regions.

## 6. Conclusion

Geochemical data indicate that the Maotan, Huayuangong, Xiangshuijian and Banshiling granites exposed along the south bank of the LYR belt, are typical A-type granites and are characterized by high Fe* ($FeO_T/(FeO_T+MgO)$), enrichments of incompatible elements (REE (except Eu), Zr, Nb and Ta), and depletion in Ba, Sr and Eu, indicating high genesis temperature, with low oxygen fugacity. These are consistent with their mantle origins. Zircon U–Pb ages of the Maotan, Huayuangong, Xiangshuijian and Banshiling granites are 125.4 Ma, 125.3 Ma, 125.4 Ma and 125.3 Ma, respectively.

A-type granites from the LYR and nearby regions consist of both $A_1$ and $A_2$ chemical subgroups, distributing in three zones, roughly parallel to each other and to a slightly older adakite belt. This can be plausibly interpreted using a ridge subduction model. The drier and hotter spreading ridge formed adakitic rocks through slab melting during subduction. The overriding mantle near the ridge was not significantly metasomatised by the subducting ridge, because limited water hosted in oceanic crust was absorbed by adakitic magmas during dehydration partial melting, such that $A_1$ granites formed subsequently during slab window opening and/or slab rollback/break-off. From the spreading ridge outwards, the oceanic crust becomes increasingly wetter and colder, consequently, dehydration induced metasomatism intensified, coupled with decreasing adakitic magmas during the subduction. As a result, the A-type granites formed during asthenosphere upwelling, changed gradually from $A_1$ chemical group to $A_2$. Further away from the ridge, the subduction angle was much steeper, and dehydration occurred early during the subduction, and thus dramatically reduced metasomatism away from the subduction zone, forming $A_1$ granites again. The distribution of $A_1$ and $A_2$ granites with slightly older adakitic rocks may be taken as discrimination indice for ridge subduction perpendicular to the subduction zone.

Supplementary materials related to this article can be found online at doi:10.1016/j.lithos.2011.09.021.

## Acknowledgment

The study is supported by a major project of the Chinese Academy of Sciences (KZCX1-YW-15) and National Natural Science Foundation of China (No. 41090374). The authors would like to thank two anonymous referees for constructive review comments, and editor Dr. Nelson Eby for constructive suggestions. Contribution No. IS-1390 from GIGCAS.

## References

Ballard, J.R., Palin, J.M., Campbell, I.H., 2002. Relative oxidation states of magmas inferred from Ce(IV)/Ce(III) in zircon: application to porphyry copper deposits of northern Chile. Contributions to Mineralogy and Petrology 144 (3), 347–364.
Belousova, E.A., Griffin, W.L., Suzanne, Y.O.R., Fisher, N.I., 2002. Igneous zircon: trace element composition as an indicator of source rock type. Contributions to Mineralogy and Petrology 143 (5), 602–622.
Bonin, B., 2007. A-type granites and related rocks: evolution of a concept, problems and prospects. Lithos 97 (1–2), 1–29.
Cao, Y., Du, Y.S., Cai, C.L., Qin, X.L., Li, S.T., Xiang, W.S., 2008. Mesozoic A-type granitoids and xenoliths in the Lujiang-Zongyang area, Anhui Province: significance in post-collisional magmatic evolution. Geological Journal of China Universities 4, 565–576 (in Chinese with English abstract).
Chang, Y.F., Liu, X.P., Wu, Y.C., 1991. The Copper–Iron Belt of the Lower and Middle Reaches of the Changjiang River. Geological Publishing House, Beijing.
Chen, J.F., Zhou, T.X., Yin, C.S., Foland, K.A., 1991. $^{40}Ar$–$^{39}Ar$ dating of several Mesozoic plutons in southeastern Zhejiang province. Acta Geologica Sinica 7 (3), 37–44 (in Chinese with English abstract).
Chen, J.F., Foland, K.A., Liu, Y.M., 1993. Precise $^{40}Ar$–$^{39}Ar$ dating of the Suzhou composite granite. Acta Geologica Sinica 9 (01), 77–85 (in Chinese with English abstract).
Chen, J.F., Yan, J., Xie, Z., Xu, X., Xing, F., 2001. Nd and Sr isotopic compositions of igneous rocks from the Lower Yangtze region in eastern China: constraints on sources. Physics and Chemistry of the Earth Part A—Solid Earth and Geodesy 26 (9–10), 719–731.
Cole, R.B., Stewart, B.W., 2009. Continental margin volcanism at sites of spreading ridge subduction: examples from southern Alaska and western California. Tectonophysics 464 (1–4), 118–136.
Deng, J.F., Dai, S.Q., Zhao, H.L., Du, J.G., 2002. Recognition of magma–fluid–metallogenic system and subsystem in the Tongling Cu–Au (Ag) metallogenic area. Mineralium Deposita 21 (4), 317–322.
Ding, X., Lundstrom, C., Huang, F., Li, J., Zhang, Z.M., Sun, X.M., Liang, J.L., Sun, W.D., 2009. Natural and experimental constraints on formation of the continental crust based on niobium–tantalum fractionation. International Geology Review 51 (6), 473–501.
Du, Y.S., Cao, Y., Yuan, W.M., Lou, Y.E., Li, S.T., Lu, X., 2007. Mesozoic post-collisional to postorogenic magmatic activities and crustal interaction with mantle along the Yangtze River, Anhui province: evidence from volcanic-intrusive complexes and xenoliths. Acta Petrologica Sinica 23 (6), 1294–1302 (in Chinese with English abstract).
Eby, G.N., 1990. The A-type granitoids a review of their occurrence and chemical characteristics and speculations their petrogenesis. Lithos 26 (1–2), 115–134.
Eby, G.N., 1992. Chemical subdivision of the A-type granitoids petrogenetic and tectonic implications. Geology 20 (7), 641–644.
Fan, Y., Zhou, T.F., Yuan, F., Qian, C.C., Lu, S.M., Cooke, D., 2008. LA–ICP-MS zircon U–Pb ages of the A-type granites in the Lu-Zong (Lujiang–Zongyang) area and their geological significances. Acta Petrologica Sinica 24 (8), 1715–1724 (in Chinese with English abstract).
Foley, S., Tiepolo, M., Vannucci, R., 2002. Growth of early continental crust controlled by melting of amphibolite in subduction zones. Nature 417 (6891), 837–840.
Frost, C.D., Frost, B.R., 2011. On ferroan (A-type) granitoids: their compositional variability and modes of origin. Journal of Petrology 52 (1), 39–53.
Frost, B.R., Barnes, C.G., Collins, W.J., Arculus, R.J., Ellis, D.J., Frost, C.D., 2001. A geochemical classification for granitic rocks. Journal of Petrology 42 (11), 2033–2048.
Green, T.H., 1995. Significance of Nb/Ta as an indicator of geochimecal processes in the crust–mantle system. Chemical Geology 120 (3–4), 347–359.
Green, T.H., Pearson, N.J., 1986. Ti-rich accessory phase saturation in hydrous mafic-felsic compositions at high P, T. Chemical Geology 54 (3–4), 185–201.
Harrison, T.M., Watson, E.B., 1984. The behavior of apatite during crustal anatexis—equilibrium and kinetic considerations. Geochimica Et Cosmochimica Acta 48 (7), 1467–1477.

Hoskin, P.W.O., Black, L.P., 2000. Metamorphic zircon formation by solid-state recrystallization of protolith igneous zircon. Journal of Metamorphic Geology 18 (423–439).

Hou, Z.Q., Pan, X.F., Yang, Z.M., Qu, X.M., 2007. Porphyry Cu–(Mo–Au) deposits no related to oceanic-slab subduction: examples from Chinese porphyry deposits in continental settings. Geoscience 21 (2), 332–351 (in Chinese with English abstract).

Li, S.G., Xiao, Y.L., Liou, D., Chen, Y., Ge, N., Zhang, Z., Sun, S.-, Cong, B., Zhang, R., Hart, S.R., Wang, S., 1993. Collision of the North China and Yangtze blocks and formation of coesite-bearing eclogites; timing and processes. Chemical Geology 109 (1–4), 89–111.

Li, S.G., Jagoutz, E., Chen, Y.Z., Li, Q.L., 2000. Sm–Nd and Rb–Sr isotopic chronology and cooling history of ultrahigh pressure metamorphic rocks and their country rocks at Shuanghe in the Dabie Mountains, Central China. Geochimica et Cosmochimica Acta 64 (6), 1077–1093.

Li, X.H., Qi, C.S., Liu, Y., Liang, X.R., Tu, X.L., Xie, L.W., Yang, Y.H., 2005. Petrogenesis of the Neoproterozoic bimodal volcanic rocks along the western margin of the Yangtze Block: new constraints from Hf isotopes and Fe/Mn ratios. Chinese Science Bulletin 50 (21), 2481–2486.

Li, J.W., Zhao, X.F., Zhou, M.F., Ma, C.Q., de Souza, Z.S., Vasconcelos, P., 2009. Late Mesozoic magmatism from the Daye region, eastern China: U–Pb ages, petrogenesis, and geodynamic implications. Contributions to Mineralogy and Petrology 157 (3), 383–409.

Li, H., Zhang, H., Ling, M.X., Wang, F.Y., Ding, X., Zhou, J.B., Yang, X.Y., Tu, X.L., Sun, W.D., 2011. Geochemical and zircon U–Pb study of the Huangmeijian A-type granite: implications for geological evolution of the Lower Yangtze River belt. International Geology Review 53 (5–6), 499–525.

Liang, H.Y., Campbell, I.H., Allen, C., Sun, W.D., Liu, C.Q., Yu, H.X., Xie, Y.W., Zhang, Y.Q., 2006. Zircon $Ce^{4+}/Ce^{3+}$ ratios and ages for Yulong ore-bearing porphyries in eastern Tibet. Mineralium Deposita 41 (2), 152–159.

Liang, J.L., Ding, X., Sun, X.M., Zhang, Z.M., Zhang, H., Sun, W.D., 2009. Nb/Ta fractionation observed in eclogites from the Chinese Continental Scientific Drilling Project. Chemical Geology 268 (1–2), 27–40.

Ling, M.X., Wang, F.Y., Ding, X., Hu, Y.H., Zhou, J.B., Zartman, R.E., Yang, X.Y., Sun, W.D., 2009. Cretaceous ridge subduction along the Lower Yangtze River Belt, Eastern China. Economic Geology 104 (2), 303–321.

Ling, M.X., Wang, F.Y., Ding, X., Zhou, J.B., Sun, W.D., 2011. Different origins of adakites from the Dabie Mountains and the Lower Yangtze River belt in eastern China: geochemical constraints. International Geology Review 53 (5–6), 727–740.

Liou, J.G., Zhang, R.Y., Ernst, W.G., Liu, J., McLimans, R., 1998. Mineral parageneses in the Piampaludo eclogitic body, Gruppo di Voltri, Western Ligurian Alps. Schweizerische Mineralogische Und Petrographische Mitteilungen 78 (2), 317–335.

Liu, Y., Liu, H.C., Li, X.H., 1996. Simultaneous and precise determination of 40 trace elements in rock samples using ICP-MS. Geochimica 25 (6), 552–558 (in Chinese with English abstract).

Liu, Y.S., Hu, Z.C., Gao, S., Gunther, D., Xu, J., Gao, C.G., Chen, H.H., 2008. In situ analysis of major and trace elements of anhydrous minerals by LA–ICP-MS without applying an internal standard. Chemical Geology 257 (1–2), 34–43.

Liu, S.A., Li, S.G., He, Y.S., Huang, F., 2010a. Geochemical contrasts between early Cretaceous ore-bearing and ore-barren high-Mg adakites in central-eastern China: implications for petrogenesis and Cu–Au mineralization. Geochimica et Cosmochimica Acta 74, 7160–7178.

Liu, Y.S., Gao, S., Hu, Z.C., Gao, C.G., Zong, K.Q., Wang, D.B., 2010b. Continental and oceanic crust recycling-induced melt-peridotite interactions in the trans-north China orogen: U–Pb dating, Hf isotopes and trace elements in zircons from mantle xenoliths. Journal of Petrology 51 (1–2), 537–571.

Loiselle, M.C., Wones, D.R., 1979. Characteristics of anorogenic granites. Geological society of America abstracts with programs 11, 468.

Lou, Y.E., Du, Y.S., 2006. Characteristics and zircon SHRIMP U–Pb ages of the Mesozoic intrusive rocks in Fanchang, Anhui Province. Geochimica 35 (4), 333–345 (in Chinese with English abstract).

Manning, C.E., Bohlen, S.R., 1991. The reaction titanite + kyanite = anorthite + rutile and titanite–rutile barometry in eclogites. Contributions to Mineralogy and Petrology 109 (1), 1–9.

Mao, J.W., Wang, Y.T., Lehmann, B., Yu, J.J., Du, A.D., Mei, Y.X., Li, Y.F., Zang, W.S., Stein, H.J., Zhou, T.F., 2006. Molybdenite Re–Os and albite $^{40}Ar^{39}/Ar$ dating of Cu–Au–Mo and magnetite porphyry systems in the Yangtze River valley and metallogenic implications. Ore Geology Reviews 29 (3–4), 307–324.

Maruyama, S., Isozaki, Y., Kimura, G., Terabayashi, M., 1997. Paleogeographic maps of the Japanese Islands: plate tectonic synthesis from 750 Ma to the present. Island Arc 6 (1), 121–142.

Mcdonough, W.F., 1991. Partial melting of subducted oceanic-crust and isolation of its residual eclogitic lithology. Philosophical Transactions of the Royal Society of London Series A—Mathematical Physical and Engineering Sciences 335 (1638), 407–418.

Pan, Y.M., Dong, P., 1999. The Lower Changjiang (Yangzi/Yangtze River) metallogenic belt, east central China: intrusion- and wall rock-hosted Cu–Fe–Au, Mo, Zn, Pb, Ag deposits. Ore Geology Reviews 15 (4), 177–242.

Rudnick, R.L., Barth, M., Horn, I., McDonough, W.F., 2000. Rutile-bearing refractory eclogites: missing link between continents and depleted mantle. Science 287 (5451), 278–281.

Streckeisen, A., Le Maitre, R.W., 1979. A chemical approximation to the modal QAPF classification of igneous rocks. Neues Jahrbuch für Mineralogie, Abhandlungen 136, 169–206.

Sun, S.S., McDonough, W.F., 1989. Chemical and isotopic systematics of oceanic basalts: implications for mantle composition and processed. Magmatism in the Ocean Basins, Geological Society Special Publication (42), 313–345.

Sun, W.D., Williams, I.S., Li, S.G., 2002. Carboniferous and Triassic eclogites in the western Dabie Mountains, east-central China: evidence for protracted convergence of the North and South China Blocks. Journal of Metamorphic Geology 20 (9), 873–886.

Sun, W.D., Xie, Z., Chen, J.F., Zhang, X., Chai, Z.F., Du, A.D., Zhao, J.S., Zhang, C.H., Zhou, T.F., 2003. Os–Os dating of copper and molybdenum deposits along the middle and lower reaches of the Yangtze River, China. Economic Geology and the Bulletin of the Society of Economic Geologists 98 (1), 175–180.

Sun, W.D., Ding, X., Hu, Y.H., Li, X.H., 2007. The golden transformation of the Cretaceous plate subduction in the west Pacific. Earth and Planetary Science Letters 262 (3–4), 533–542.

Sun, W.D., Ling, M.X., Yang, X.Y., Fan, W.M., Ding, X., Liang, H.Y., 2010. Ridge subduction and porphyry copper–gold mineralization: an overview. Science China-Earth Sciences 53 (4), 475–484.

Thorkelson, D.J., Breitsprecher, K., 2005. Partial melting of slab window margins: genesis of adakitic and non-adakitic magmas. Lithos 79 (1–2), 25–41.

Tu, X.L., Zhang, H., Deng, W.F., Liang, H.Y., Liu, Y., Sun, W.D., 2011. Application of RESOlution in-situ laser ablation ICP-MS in trace element analyses. Geochimica 40 (1), 83–98 (in Chinese with English abstract).

Wang, J.M., Yang, N.Q., Li, K.Q., Ding, G.C., 1993. The metallogenesis and magmatic differentiation of Suzhou A-type granite. Acta Geologica Sinica 9 (1), 33–42 (in Chinese with English abstract).

Wang, R.C., Fontan, F., Xu, S.J., Chen, X.M., Monchoux, P., 1997. The association of columbite, tantalite and tapiolite in the Suzhou granite, China. The Canadian Mineralogist 35, 699–706.

Wang, Q., Xu, J.F., Zhao, Z.H., Bao, Z.W., Xu, W., Xiong, X.L., 2004. Cretaceous high-potassium intrusive rocks in the Yueshan–Hongzhen area of east China: adakites in an extensional tectonic regime within a continent. Geochemical Journal 38 (5), 417–434.

Wang, Q., Wyman, D.A., Xu, J.F., Zhao, Z.H., Jian, P., Xiong, X.L., Bao, Z.W., Li, C.F., Bai, Z.H., 2006. Petrogenesis of Cretaceous adakitic and shoshonitic igneous rocks in the Luzong area, Anhui Province (eastern China): implications for geodynamics and Cu–Au mineralization. Lithos 89, 424–446.

Wang, Q., Wyman, D.A., Xu, J.F., Zhao, Z.H., Jian, P., Zi, F., 2007. Partial melting of thickened or delaminated lower crust in the middle of eastern China: implications for Cu–Au mineralization. Journal of Geology 115 (2), 149–161.

Wang, F.Y., Ling, M.X., Ding, X., Hu, Y.H., Zhou, J.B., Yang, X.Y., Liang, H.Y., Fan, W.M., Sun, W.D., 2011. Mesozoic large magmatic events and mineralization in SE China: oblique subduction of the Pacific plate. International Geology Review 53 (5–6), 704–726.

Watson, E.B., Wark, D.A., Thomas, J.B., 2006. Crystallization thermometers for zircon and rutile. Contributions to Mineralogy and Petrology 151 (4), 413–433.

Wong, J., Sun, M., Xing, G.F., Li, X.H., Zhao, G.C., Wong, K., Yuan, C., Xia, X.P., Li, L.M., Wu, F.Y., 2009. Geochemical and zircon U–Pb and Hf isotopic study of the Baijuhuajian metaluminous A-type granite: extension at 125–100 Ma and its tectonic significance for South China. Lithos 112 (3–4), 289–305.

Wu, C.L., Zhou, X.R., 1998. A-type granites in Maotan, Anhui. Acta Geologica Sinica 72 (3), 237–248 (in Chinese with English abstract).

Xiao, Y.L., Sun, W.D., Hoefs, J., Simon, K., Zhang, Z.M., Li, S.G., Hofmann, A.W., 2006. Making continental crust through slab melting: constraints from niobium–tantalum fractionation in UHP metamorphic rutile. Geochimica Et Cosmochimica Acta 70 (18), 4770–4782.

Xie, G.Q., Mao, J.W., Li, R.L., Zhou, S.D., Ye, H.S., Yan, Q.R., Zhang, Z.S., 2006. SHRIMP zircon U–Pb dating for volcanic rocks of the Dasi Formation in southeast Hubei Province, middle–lower reaches of the Yangtze River and its implications. Chinese Science Bulletin 51 (24), 3000–3009.

Xie, G.Q., Mao, J.W., Li, R.L., Qu, W.J., Pirajno, F., Du, A.D., 2007. Re–Os molybdenite and Ar–Ar phlogopite dating of Cu–Fe–Au–Mo (W) deposits in southeastern Hubei, China. Mineralogy and Petrology 90 (3–4), 249–270.

Xie, J.C., Yang, X.Y., Du, J.G., Sun, W.D., 2008. Zircon U–Pb geochronology of the Mesozoic intrusive rocks in the Tongling region: implications for copper–gold mineralization. Acta Petrologica Sinica 24 (8), 1782–1800 (in Chinese with English abstract).

Xie, J.C., Yang, X.Y., Sun, W.D., Du, J.G., Xu, W., Wu, L.B., Wang, K.Y., 2009. Geochronological and geochemical constrains on formation of the Tongling metal deposits, middle Yangtze metallogenic belt, east-central China. International Geology Review 51 (5), 388–421.

Xing, F.M., 1999. The magmatic metallogenetic belt around the Yangtze River in Anhui. Geology of Anhui 9 (4), 272–279 (in Chinese with English abstract).

Xing, F.M., Xu, X., 1994. Two A-type granite belts from Anhui. Chinese Journal of Geochemistry 13 (4), 340–354 (in Chinese with English abstract).

Xing, F.M., Xu, X., 1995. The essential features of magmatic rocks along the Yangtze River in Anhui province. Acta Petrologica Sinica 11 (4), 409–422 (in Chinese with English abstract).

Xiong, X.L., 2006. Trace element evidence for growth of early continental crust by melting of rutile-bearing hydrous eclogite. Geology 34 (11), 945–948.

Xiong, X.L., Adam, J., Green, T.H., 2005. Rutile stability and rutile/melt HFSE partitioning during partial melting of hydrous basalt: implications for TTG genesis. Chemical Geology 218 (3–4), 339–359.

Xiong, X.L., Keppler, H., Audetat, A., Gudfinnsson, G., Sun, W.D., Song, M.S., Xiao, W.S., Yuan, L., 2009. Experimental constraints on rutile saturation during partial melting of metabasalt at the amphibolite to eclogite transition, with applications to TTG genesis. American Mineralogist 94 (8–9), 1175–1186.

Xiong, X.L., Keppler, H., Audetat, A., Ni, H.W., Sun, W.D., Li, Y.A., 2011. Partitioning of Nb and Ta between rutile and felsic melt and the fractionation of Nb/Ta during partial melting of hydrous metabasalt. Geochimica et Cosmochimica Acta 75 (7), 1673–1692.

Xu, J.F., Shinjo, R., Defant, M.J., Wang, Q., Rapp, R.P., 2002. Origin of Mesozoic adakitic intrusive rocks in the Ningzhen area of east China: partial melting of delaminated lower continental crust? Geology 30 (12), 1111–1114.

Xue, H.M., Wang, Y., Ma, F., Wang, C., Wang, D., Zuo, Y.L., 2009. The Huangshan A-type granites with tetrad REE: constraints on Mesozoic lithospheric thinning of the southeastern Yangtze craton? Acta Geologica Sinica 83 (2), 247–259 (in Chinese with English abstract).

Yang, X.Y., Zheng, Y.F., Xiao, Y.L., Du, J.G., Sun, W.D., 2007. $^{40}Ar/^{39}Ar$ dating of the Shaxi porphyry Cu–Au deposit in the southern Tan–Lu fault zone, Anhui Province. Acta Geologica Sinica-English Edition 81 (3), 477–487.

Yang, X.Y., Yang, X.M., Zhang, Z.W., Chi, Y.Y., Yu, L.F., Zhang, Q.M., 2011. A porphyritic copper (gold) ore-forming model for the Shaxi–Changpushan district, Lower Yangtze metallogenic belt, China: geological and geochemical constraints. International Geology Review 53 (5–6), 580–611.

Yu, L.F., Yang, X.Y., Sun, W.D., Chi, Y.Y., Zhang, Q.M., 2008. The adakite and mineralization of the Shaxi porphyry copper–gold deposit, Central Anhui. Geology in China 6, 1150–1161 (in Chinese with English abstract).

Zhai, Y.S., Yao, S.Z., Lin, X.D., 1992. Metallogeny of Iron and Copper (Gold) Deposits in the Middle–Lower Reaches of Yangtze River. Geological Publishing House, Beijing.

Zhai, Y.S., Xiong, Y.L., Yao, S.Z., Lin, X.D., 1996. Metallogeny of copper and iron deposits in the Eastern Yangtze Craton, east-central China. Ore Geology Reviews 11, 229–248.

Zhang, B.D., Zhang, F.S., Ni, Q.S., Chen, P.R., Zhai, J.P., Shen, W.Z., 1988. Geology geochemistry and genisis discution of quartz syenite in Anlu belt. Acta Petrologica Sinica 3, 1–12 (in Chinese with English abstract).

Zhang, Q., Wang, Y., Qian, Q., Yang, J.H., Wang, Y.L., Zhao, T.P., Guo, G.J., 2001. The characteristics and tectonic–metallogenic significances of the adakites in Yanshan period from eastern China. Acta Petrologica Sinica 17 (2), 236–244 (in Chinese with English abstract).

Zhang, Q., Qin, K.Z., Wang, Y., Zhang, F.Q., Liu, H.T., Wang, Y., 2004. Study on adakite broadened to challenge the Cu and Au exploration in China. Acta Petrologica Sinica 20 (2), 195–204 (in Chinese with English abstract).

Zhang, S., Zhang, Z.C., Ai, Y., Yuan, W.M., Ma, L.T., 2009. The petrology, mineralogy and geochemistry study of the Huangshan granite intrusion in Anhui Province. Acta Petrologica Sinica 25 (1), 25–38 (in Chinese with English abstract).

Zheng, Y.F., Fu, B., Gong, B., 1995. The thermal history of the Huangmeijian intrusion in Anhui and its relation to mineralization: isotopic evidence. Acta Geologica Sinica 69 (4), 337–348.

Zheng, Y.F., Fu, B., Gong, B., Li, L., 2003. Stable isotope geochemistry of ultrahigh pressure metamorphic rocks from the Dabie–Sulu orogen in China: implications for geodynamics and fluid regime. Earth-Science Reviews 62 (1–2), 105–161.

Zhou, X.M., Zou, H.B., Yang, J.D., Wang, Y.X., 1990. Sm–Nd isochronous age of Fuchuan ophiolite suite in Shexian County, Anhui Province and its geological significance. Chinese Science Bulletin 35 (3), 208–212.